Applied Catalysis B: Environmental 134–135 (2013) 381–388

Contents lists available at SciVerse ScienceDirect

Applied Catalysis B: Environmental

journal homepage: www.elsevier.com/locate/apcatb

# Magnesia modified H-ZSM-5 as an efficient acidic catalyst for steam reforming of dimethyl ether

Xu Long[a], Qijian Zhang[b], Zhao-Tie Liu[a], Ping Qi[b], Jian Lu[a], Zhong-Wen Liu[a,*]

[a] Key Laboratory of Applied Surface and Colloid Chemistry (MOE), School of Chemistry & Chemical Engineering, Shaanxi Normal University, Xi'an 710062, China
[b] School of Chemical and Environmental Engineering, Liaoning University of Technology, Jinzhou 121001, China

ARTICLE INFO

*Article history:*
Received 5 August 2012
Received in revised form
12 December 2012
Accepted 20 January 2013
Available online 26 January 2013

*Keywords:*
Hydrogen production
Steam reforming
Dimethyl ether
Magnesia
ZSM-5

ABSTRACT

To develop an efficient acidic catalyst for steam reforming of dimethyl ether (DME), H-ZSM-5 was modified with a series amount of MgO (0–8.16 wt.%) via the incipient impregnation method by using $Mg(NO_3)_2$ as a precursor. Irrespective of the MgO loadings studied, it was highly dispersed over H-ZSM-5, and very limited impact on the structure and crystallinity of the zeolite was unambiguously revealed by the techniques of XRD, FT-IR, and $N_2$ adsorption at low temperatures. On the contrary, significant effects of MgO on the acidity of H-ZSM-5, especially the stronger acidic sites, were clearly manifested from the temperature-programmed desorption of ammonia ($NH_3$-TPD). The amount of the stronger acidic sites was sharply decreased after loading 0.61 wt.% MgO on H-ZSM-5, and it was continuously decreased when the MgO loading was further increased until 8.16 wt.%. In contrast, the maximum amount of weaker acidic sites was observed between 1.41 and 2.92 wt.% MgO loaded samples. The MgO-modified H-ZSM-5 physically mixed with a commercial $Cu/ZnO/Al_2O_3$ was investigated as a bifunctional catalyst for steam reforming of DME (SRD). The reaction was performed in a fixed-bed reactor under the conditions of $T = 290\,^{\circ}C$, $P = 1$ atm, and GHSV = 4000 $h^{-1}$. SRD results indicate that the DME conversion, $H_2$ yield, and selectivity of the carbon-containing products were strongly dependent on the MgO loadings over H-ZSM-5, and the highest $H_2$ yield of about 93% was achieved over the bifunctional catalyst by using 1.98 wt.% MgO modified H-ZSM-5 as a solid acid. Together with the reaction and characterization results of the $Mg^{2+}$-exchanged H-ZSM-5, the property of the stronger acidic sites over the MgO-modified H-ZSM-5 was revealed to be a crucial factor in determining the SRD performance of the bifunctional catalyst. The simple impregnation procedure and the high efficiency in versatile tailoring the acidity make MgO-modified H-ZSM-5 a practical, highly efficient, and promising solid acid for hydrogen production via SRD.



## 1. Introduction

The proton exchange membrane fuel cell (PEMFC), which is characterized by environmental benignity, low operating temperature, high efficiency, and high reliability, has been recognized as a desirable power generation system for portable devices and electric vehicles [1]. The on-board steam reforming of hydrogen-rich compounds, such as hydrocarbons (methane, liquefied petroleum gas (LPG), and gasoline) and oxygenates (methanol and ethanol) is quantitatively investigated as an attractive route to supply hydrogen for fuel cells, especially for PEMFC [2,3]. However, the on-board generation of hydrogen from these hydrogen carriers is still not satisfactory in the aspects of delivering infrastructure (a pump generally required for liquid feedstock of gasoline, ethanol, etc.), toxicity (harmful methanol), and reforming conditions (generally above 600 °C for the reforming of hydrocarbons) [2–4]. Recently, dimethyl ether (DME) is considered to be a suitable feedstock for hydrogen generation via steam reforming technology because of its non-toxicity or harmlessness, higher hydrogen content (13.0 wt.%), gas-like property and liquid-storage density, and available handling infrastructure (similar to LPG) [5]. Moreover, the steam reforming of DME (SRD) can be carried out at low reforming temperatures of 200–400 °C. Thus, after the pioneering work of Sobyanin at the beginning of the 21st century [6,7], quite a few works on SRD including thermodynamics analyses [8–11] and catalyst development have been reported in recent years [12–18]. Although noble metals supported on oxides are reported active for SRD [19], to date, the basic idea for designing catalyst and interpreting the experimental data is overwhelmingly based on the two-step mechanism proposed by Sobyanin and co-workers [7] as

* Corresponding author at: No. 199, South Chang'an Road, School of Chemistry & Chemical Engineering, Shaanxi Normal University, Xi'an 710062, China.
Tel.: +86 29 8153 0801; fax: +86 29 8153 0727.
*E-mail address:* zwliu@snnu.edu.cn (Z.-W. Liu).

0926-3373/$ – see front matter © 2013 Elsevier B.V. All rights reserved.
http://dx.doi.org/10.1016/j.apcatb.2013.01.034

shown in Eqs. (1)–(3). Moreover, side reactions (Eqs. (4)–(9)) may also occur, the extent of which is dependent on the catalyst system and reaction parameters.

$$CH_3OCH_3 + 3H_2O = 2CO_2 + 6H_2 \quad \Delta H^\circ = 135\,kJ\,mol^{-1} \quad SRD \quad (1)$$

$$CH_3OCH_3 + H_2O = 2CH_3OH \quad \Delta H^\circ = 37\,kJ\,mol^{-1}$$

DME hydrolysis (2)

$$CH_3OH + H_2O = CO_2 + 3H_2 \quad \Delta H^\circ = 49\,kJ\,mol^{-1} \quad SRM \quad (3)$$

$$CO_2 + H_2 = CO + H_2O \quad \text{Reverse water gas shift reaction (RWGS)} \quad (4)$$

$$CO + 3H_2 = CH_4 + H_2O \quad \text{Methanation reaction} \quad (5)$$

$$CH_3OCH_3 \rightarrow CH_4 + CO + H_2 \quad \text{DME decomposition} \quad (6)$$

$$2CO = C + CO_2 \quad \text{Boudouard reaction} \quad (7)$$

$$CH_3OCH_3 \rightarrow \text{hydrocarbons} \quad DTH \quad (8)$$

$$CH_3OH \rightarrow \text{hydrocarbons} \quad MTH \quad (9)$$

Although the DME hydrolysis (Eq. (2)) is thermodynamically limited, the removal of the intermediate product of methanol via steam reforming (SRM) makes SRD favorable at lower temperatures of 200–400 °C. Kinetically, high hydrogen yields can be reasonably expected provided that the reaction rates of the DME hydrolysis and SRM are sufficiently high and well matched. Thus, different bifunctional catalyst systems composed of solid acid for DME hydrolysis and metal-supported oxide for SRM are investigated [12–18]. In the case of SRM, although precious metals show better performance [20–23], sufficiently active and cheap Cu-based oxides are more preferred. Thus, the optimization of Cu-based oxides in the aspects of compositions and preparation methods is extensively studied [12,15,16,24–27,29–33]. When the DME hydrolysis is concerned, alumina [7,14–18,23–30,34–40], zeolites [32,33,35–42], and super acids such as $WO_3/ZrO_2$ [22,31,32,43,44] are commonly used as a solid acid catalyst. The shortcoming of alumina for DME hydrolysis is to require a higher reaction temperature greater than 300 °C [15,16,18,24–30,35–37], at which the Cu-based catalyst can be obviously sintered. However, the stability of the alumina based bifunctional catalyst is high as a result of the low coke deposition [12,24,39]. Indeed, zeolites such as ZSM-5 as a solid acid catalyst are active enough for the DME hydrolysis at temperatures below 300 °C, which is comparable with the working temperature of the Cu-based catalyst such as $Cu/ZnO/Al_2O_3$. However, since the stronger acidic sites over zeolites are favorable for the formation of hydrocarbons (Eqs. (8)–(9)), coke is always deposited over the zeolites at the working temperatures of SRD. Consequently, clear catalyst deactivation and relatively low hydrogen selectivity are generally observed for SRD over a bifunctional catalyst composed of zeolite and Cu-based oxides [45,46].

Thus, by inheriting the merits but overcoming the respective shortcomings of alumina and zeolites, i.e., removing the stronger acidic sites but keeping the weaker acidic sites over zeolites, an efficient solid acid catalyst for SRD can be reasonably expected. As a common knowledge, the acidity of zeolites is closely related to the framework structure and the content of the framework aluminum cations. Indeed, zeolites having different framework structures and $SiO_2/Al_2O_3$ ratios show clear impact on the performance of SRD over composite catalyst of zeolite and Cu-based oxides [36,39,40]. However, without significantly changing the properties of the weaker acidic sites, it is difficult to selectively remove the stronger acidic sites by just varying the framework structure and/or $SiO_2/Al_2O_3$ ratio of zeolites. More recently, a clearly improved stability of the catalyst for SRD is observed when the H-ZSM-5 treated with NaOH solution is used as an acidic catalyst [46]. However, after treating H-ZSM-5 with NaOH solution, DME conversion and $H_2$ yield are apparently decreased as a result of the simultaneously decreased quantities of both stronger and weaker acidic sites over the zeolite [46]. Alternatively, the introduction of basic oxides such as MgO, $La_2O_3$ has been investigated to tailor the acidity and porous properties of zeolites for catalyzing a number of reactions [47–53]. Moreover, it is possible to selectively poison the stronger acidic sites in zeolites provided that suitable content and introduction method of basic oxides are applied [51–53]. However, the zeolite modified with basic oxides as a solid acid catalyst for SRD is not reported to date.

In this work, we demonstrate that an efficient solid acid catalyst for SRD can be obtained by modifying H-ZSM-5 with MgO, and its content and introduction method are optimized. The MgO-modified H-ZSM-5 physically mixed with a commercial $Cu/ZnO/Al_2O_3$ was investigated as a bifunctional catalyst for SRD, and great impacts of MgO on the performance of the catalyst was clearly manifested. Over the optimized catalyst, about 93% hydrogen yield was obtained and the side reactions for the formation of hydrocarbons were greatly inhibited. Significantly, our results reveal that the MgO-modified H-ZSM-5 via a simple impregnation method can be a highly efficient and promising solid acid for SRD.

## 2. Experimental

### 2.1. Preparation of MgO-modified H-ZSM-5

The commercial H-ZSM-5 ($SiO_2/Al_2O_3$ molar ratio of 25, Nankai University Catalyst Co., Ltd.) was calcined at 550 °C for 3 h to remove any possible volatiles. Then, the incipient impregnation method was applied for the modification of H-ZSM-5 with different contents of MgO by using magnesium nitrate as a precursor. After drying at 120 °C for 12 h, the samples were calcined in air at 550 °C for 3 h, and H-ZSM-5 modified with different amounts of MgO samples were obtained. After digesting the samples in a mixed solution of HF and $HNO_3$, the MgO content over the samples was determined to be 0.61, 1.41, 1.98, 2.92, 3.71, 5.08, 6.47, and 8.16 wt.%, respectively, by using inductively coupled plasma (ICP) optical emission spectroscopy.

### 2.2. Preparation of hybrid catalysts

The bifunctional catalyst for SRD was a physical mixture of the MgO-modified H-ZSM-5 and a commercial $Cu/ZnO/Al_2O_3$ (Type C207-G, Changshu Kaituo Catalyst Co., Ltd.). The weight ratio of the two components was set to be 1. To make each component further pulverized and thoroughly mixed, the mixture was co-grinded for about 10 min, and was then treated for 20 min under ultrasonic conditions (100 W, 40 kHz) in ethanol. After evaporating the ethanol and drying at 80 °C for 2 h, the mixture was subject to pressure-molding, crushing, and sieving. Finally, 40–60 mesh particles were used for the reaction test.

### 2.3. SRD procedure and product analysis

The catalytic reaction was performed in a quartz tube (i.d. = 8.0 mm), and the loading of the hybrid catalyst was 0.9 g. To activate $Cu/ZnO/Al_2O_3$, the hybrid catalyst was reduced in a diluted $H_2$ (10 vol.% $H_2/N_2$). After the temperature was reached to be 290 °C, SRD was started at a $DME/H_2O/N_2$ = 1/4/5 (molar ratio). The $N_2$ and DME with desired flow rates were fed by mass flow controllers, and the deionized water was injected with an HPLC syringe pump and evaporated at 150 °C.

The effluent products were analyzed by an on-line gas chromatography (GC-9560, Huaai chromatographic analysis Co., Ltd.).

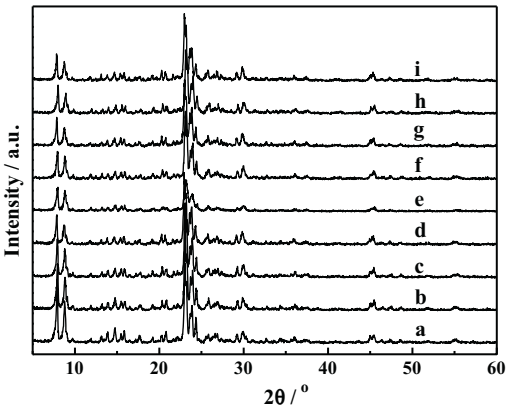


**Fig. 1.** XRD patterns of H-ZSM-5 (a) and the H-ZSM-5 modified with MgO at a weight content of 0.61% (b), 1.41% (c), 1.98% (d), 2.92% (e), 3.71% (f), 5.08% (g), 6.47% (h), and 8.16% (i), respectively.

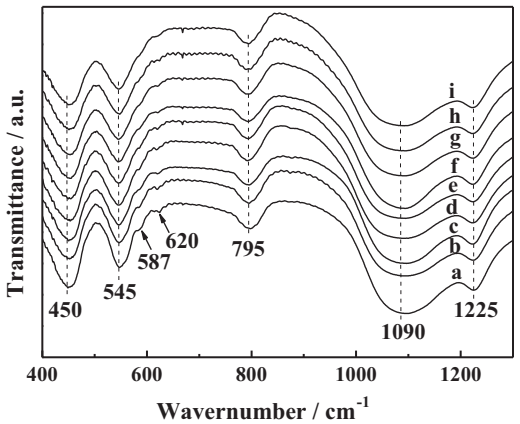


**Fig. 2.** FT-IR spectra of the H-ZSM-5 (a) and the H-ZSM-5 modified with MgO at a weight content of 0.61% (b), 1.41% (c), 1.98% (d), 2.92% (e), 3.71% (f), 5.08% (g), 6.47% (h), and 8.16% (i), respectively.

The details for GC analysis and the calculation of DME conversion, $H_2$ yield, and selectivity of carbon-containing products have been described in our previous work [42].

### 2.4. Characterizations

Powder X-ray diffraction (XRD) patterns of the H-ZSM-5 modified by different amounts of MgO were recorded at room temperature on a Rigaku D/Max-3c instrument using monochromatized Cu/$K_\alpha$ radiation (40 kV, 30 mA). All the samples were scanned from 5° to 60° (2$\theta$) at a speed of 8° per minute.

Fourier transform infrared spectroscopy (FT-IR) spectra were obtained on a Nicolet Avatar 360 spectrometer at a resolution of 1 $cm^{-1}$. After drying at 300 °C, the samples were compressed into pellets using the KBr pressed disk technique (1 wt.% sample).

$N_2$ adsorption–desorption isotherms were measured with a BELSORP-max instrument at −196 °C. Before analyses, the samples (~150 mg) were degassed at 350 °C for 12 h. The specific surface area was calculated using the BET method, and the distribution of the micropore size was determined based on the H-K method.

The acidity of the H-ZSM-5 derived samples was characterized by temperature-programmed desorption of ammonia ($NH_3$-TPD) on a Micromeritics Autochem 2920 instrument. For each test, the sample (0.05 g) was loaded. After flushing with a He flow at 800 °C for 1 h, the temperature was decreased to 120 °C under a He flow. Then, diluted $NH_3$ with a flow rate of 25 $cm^3$ $min^{-1}$ was switched, and the adsorption of $NH_3$ was carried out at 120 °C for 30 min. After this, it was flushed with a He flow for 2 h to remove the physically adsorbed $NH_3$. Finally, $NH_3$-TPD was performed up to 800 °C at a heating rate of 10 °C per minute under a He flow of 25 $cm^3$ $min^{-1}$.

## 3. Results and discussion

### 3.1. Structural and textural properties of MgO-modified H-ZSM-5

#### 3.1.1. Structural properties

The XRD patterns of H-ZSM-5 modified with different amounts of MgO are given in Fig. 1. As indicated from the characteristic diffractions of MFI framework, the raw H-ZSM-5 was well crystallized. After introducing as high as 8.16 wt.% MgO, all the XRD peaks of H-ZSM-5 were still clearly observable, indicating that the framework structure of ZSM-5 is well preserved. When the peak intensities were examined, irrespective of the MgO content over H-ZSM-5, negligible changes were found for all the XRD diffractions at $2\theta > 10°$. However, the intensity of the two peaks at ~7.9° (0 1 1) and ~8.8° (0 2 0) was clearly decreased with increasing the content of MgO in H-ZSM-5 from 0 to 2.92 wt.%, and was leveled off when the content of MgO was further increased until 8.16 wt.%. Thus, after modification of H-ZSM-5 with MgO at loadings between 0.61 and 8.16 wt.%, the MFI framework of ZSM-5 was still well retained.

When magnesium species were concerned, as indicated in Fig. 1, no XRD peaks assigned to crystalline magnesia were found over all the MgO modified samples. Moreover, phases due to mixed oxides such as $MgAl_2O_4$ were not detected by XRD, which is consistent with the relatively lower calcination temperature of 550 °C. As reported in many works [47–53], there is no doubt that the impregnated magnesium nitrate was transferred into MgO under the present conditions. Thus, irrespective of the MgO loadings, highly dispersed MgO over H-ZSM-5 can be suggested.

It has been reported that MgO is prone to disperse over $Al_2O_3$, and the threshold monolayer capacity is determined to be 0.084 g MgO per 100 $m^2$ support [54,55]. Moreover, the monolayer dispersion of MgO over H-ZSM-5 ($SiO_2/Al_2O_3$ = 38) has been reported to be 0.12 g MgO/g H-ZSM-5 [56,57]. However, crystalline MgO was detected by XRD when 10 wt.% MgO was loaded over H-ZSM-5 ($SiO_2/Al_2O_3$ = 76) [53]. In our case, there were still no crystalline MgO detected by XRD even at a MgO loading of 8.16 wt.%, corresponding to 0.02 g MgO per 100 $m^2$ H-ZSM-5. Considering the varied $SiO_2/Al_2O_3$ ratios and the BET surface areas of ZSM-5, our results are consistent to those of the references [53,54,56]. Thus, it can be concluded that MgO is highly dispersed over H-ZSM-5 for all the samples. As a result of the low external surface area, MgO is expected to be mainly located in the internal surfaces of H-ZSM-5, i.e., inside the channel and the channel crossing. This is well supported from the changing pattern of the intensities of the (0 1 1) and (0 2 0) diffractions, i.e., firstly decreased and then leveled off with increasing MgO content, because that the decreased intensity of the XRD peaks below 10° (2$\theta$) is indicative of the presence of any species inside the channels of ZSM-5 [54,58].

#### 3.1.2. Crystallinity

To further probe the impact of MgO on the crystallinity of H-ZSM-5, FT-IR spectra at the lattice regions of 400–1400 $cm^{-1}$, which characterize the vibrations of $TO_4$ (T = Si and Al) tetrahedra [56,59,60], were recorded, and the results are shown in Fig. 2. According to the reported results [60], the main IR bands of H-ZSM-5 at 450, 545, 795, and 1090 $cm^{-1}$ can be assigned to the bending of the $TO_4$ tetrahedra, the vibration of the structurally sensitive double five-member ring, and the symmetric and asymmetric stretching vibrations of the T—O—T linkages, respectively. In comparison with the parent H-ZSM-5, no new IR bands appeared for all the MgO-modified samples. Moreover, independent on the

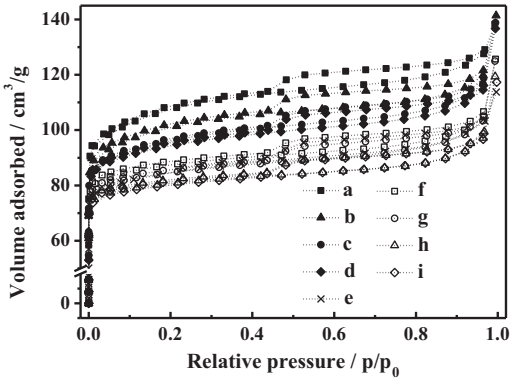


**Fig. 3.** $N_2$ adsorption–desorption isotherms of H-ZSM-5 (a) and the H-ZSM-5 modified with MgO at a weight content of 0.61% (b), 1.41% (c), 1.98% (d), 2.92% (e), 3.71% (f), 5.08% (g), 6.47% (h), and 8.16% (i), respectively.

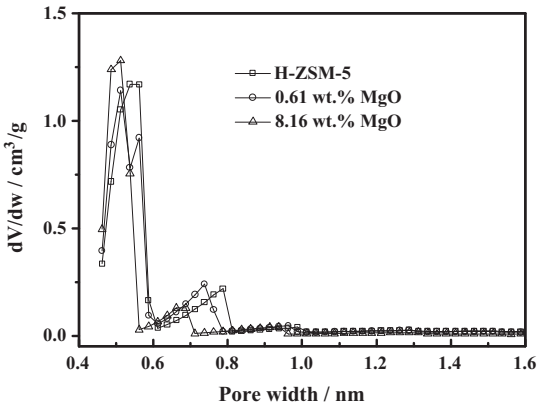


**Fig. 4.** Pore size distributions determined by the H-K method for H-ZSM-5 modified with different amounts of MgO.

MgO loadings, both the peak position and the intensity of the main IR absorptions observed for H-ZSM-5 were kept constant for all the MgO-containing samples. This indicates that the influence of MgO on the crystallinity of H-ZSM-5 is very limited.

The ratio of the 545 to 450 $cm^{-1}$ bands in intensity ($A_{545}/A_{450}$) is generally used as an index to characterize the crystallinity of zeolites [59,60], and $A_{545}/A_{450}$ of 0.7 is reported for a well crystallized ZSM-5 [59]. The $A_{545}/A_{450}$ calculated for H-ZSM-5 was 0.77, indicative of its high crystallinity. Moreover, as indicated in Fig. 2, the intensity of the 545 and 450 $cm^{-1}$ bands kept almost constant when the MgO content over H-ZSM-5 was increased from 0 to 8.16 wt.%, leading to the almost invariant $A_{545}/A_{450}$ between 0.77 and 0.84 for all the samples. Thus, the impact of MgO on the crystallinity of ZSM-5 framework is negligible. This is further supported from that the intensity of the two small shoulder peaks at 587 and 620 $cm^{-1}$, which are associated with the vibration of the double five-member ring [60], was only slightly decreased with increasing the MgO loading from 0 to 8.16 wt.%. Therefore, it is clear that the framework of H-ZSM-5 remained intact even after impregnating with as high as 8.16 wt.% MgO, which is well agreeable with the XRD results.

### 3.1.3. Textural properties

Fig. 3 shows the $N_2$ adsorption–desorption isotherms of the H-ZSM-5 derived samples. Irrespective of the MgO contents in H-ZSM-5, all the samples presented a type I isotherm, which is typically observed for microporous materials. In the case of the parent H-ZSM-5, the volume of the adsorbed $N_2$ was sharply increased with increasing $p/p_0$ until ~0.05, indicative of the presence of many small micropores. The amount of the adsorbed $N_2$ was only slightly increased when $p/p_0$ was further increased to be ~0.9. Moreover, only a small H4 hysteresis loop was observed. Thus, the volume of the mesopores was very limited, which can be clearly reflected from the pore size distributions determined by the BJH method (not shown). In the cases of the MgO containing samples, quite similar isotherms to that of H-ZSM-5 were observed in the regions of $p/p_0 > 0.2$, indicating the very limited amount of mesopores. However, the volume of the adsorbed $N_2$ at $p/p_0 < 0.1$ was continuously decreased with increasing the MgO loading over H-ZSM-5. This indicates that the micropore volume was gradually decreased with increasing MgO content. The thus mentioned characteristics were quantitatively reflected from the calculated data based on the isotherms. As shown in Table 1, both the BET surface area and pore volume, which are contributed overwhelmingly by the micropores, were monotonically decreased with increasing the content of MgO over H-ZSM-5. Furthermore, a good linearity can be observed if the surface area or pore volume is plotted against the MgO loadings. This can be well explained as the high dispersion of the very small MgO particles on the channel walls of H-ZSM-5, which is well agreeable with the distributions of micropores determined by the H-K method (Fig. 4) and the intensity changes of the XRD diffractions below 10° (Fig. 1). Thus, even as high as 8.16 wt.% MgO was loaded on H-ZSM-5, it is still highly dispersed on the surfaces of the zeolite.

### 3.2. Acidic properties of MgO-modified H-ZSM-5

The acidity of the parent H-ZSM-5 and MgO loaded samples was determined by $NH_3$-TPD, and the results are given in Fig. 5. In the case of the parent H-ZSM-5, two $NH_3$ desorption peaks at maximum temperatures of about 200 and 360 °C were clearly observed, which can be reasonably ascribed to weaker and stronger acidic sites, respectively [42]. After impregnating 0.61 wt.% MgO over H-ZSM-5, the intensity of the low-temperature peak was slightly increased and the intensity of the high-temperature peak was significantly decreased although the maximum temperatures were

**Table 1**
The calculated textural properties of the H-ZSM-5 modified with different amounts of MgO.

| MgO loaded on H-ZSM-5 (wt.%) | BET surface area ($m^2/g$) | Micropore surface area ($m^2/g$)[a] | Total pore volume ($cm^3/g$) | Micropore volume ($cm^3/g$)[a] |
|---|---|---|---|---|
| 0 | 415.0 | 402.2 | 0.241 | 0.181 |
| 0.61 | 402.6 | 390.3 | 0.217 | 0.161 |
| 1.41 | 360.4 | 346.3 | 0.210 | 0.153 |
| 1.98 | 354.6 | 341.3 | 0.207 | 0.151 |
| 2.92 | 346.5 | 335.5 | 0.198 | 0.136 |
| 3.71 | 337.8 | 325.0 | 0.190 | 0.136 |
| 5.08 | 326.8 | 313.4 | 0.190 | 0.133 |
| 6.47 | 313.1 | 300.9 | 0.180 | 0.125 |
| 8.16 | 310.4 | 298.4 | 0.174 | 0.125 |

[a] Determined by *t*-plot method.

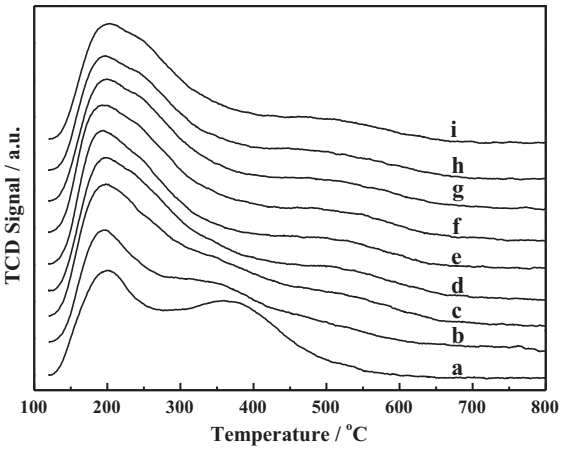


**Fig. 5.** $NH_3$-TPD patterns of H-ZSM-5 (a) and the H-ZSM-5 modified with MgO at a weight content of 0.61% (b), 1.41% (c), 1.98% (d), 2.92% (e), 3.71% (f), 5.08% (g), 6.47% (h), and 8.16% (i), respectively.

kept unchanged. This indicates that the amount of the stronger acidic sites over H-ZSM-5 was decreased significantly together with a slight increase in the amount of the weaker acidic sites. When the content of MgO was further increased to be 1.41 wt.%, the peak due to the stronger acidic sites was immerged as a shoulder of the low-temperature peak, in which its intensity was further increased. Moreover, relatively small changes were clearly observed for the $NH_3$-TPD patterns when the MgO loading was further increased until 8.16 wt.%. Thus, impregnating MgO over H-ZSM-5 is an effective method to eliminate the stronger acidic sites over the zeolite, which is generally agreeable with previous reports [51–53,61].

To quantify these changes, the $NH_3$-TPD peaks were integrated, and the following characteristics were observed: (1) the amount of stronger acidic sites were continuously decreased with increasing the MgO loadings from 0 to 8.16 wt.%; (2) weaker acidic sites were generated after impregnating MgO over H-ZSM-5, and the maximum was obtained for the samples with MgO loadings of 1.41–2.92 wt.%. Moreover, as indicated from the unchanged peak temperatures, the strength of the weaker and stronger acidic sites was retained almost the same irrespective of MgO loadings. Except the maximum of the weaker acidic sites, these observations are in good agreement with the reported results of H-ZSM-5 modified by MgO via a solid reaction method [61]. In addition, similar observations were obtained over Fe/ZSM-5 [62], alkaline earth oxide modified ZSM-5 [50], and MgO modified beta zeolite [52] and MCM-22 [51]. On the contrary, the strength of the weaker acidic sites over H-ZSM-5 ($SiO_2/Al_2O_3$ = 76) was found to be increased at a higher MgO loading (≥2.5 wt.%) but kept the same at a MgO loading of 0.5 wt.% [53]. This slight difference can be reasonably ascribed to the varied crystalline properties and $SiO_2/Al_2O_3$ ratios of H-ZSM-5, and the properties of MgO since crystalline MgO was detected by XRD for the 10 wt.% MgO loaded sample [53].

Concerning the nature of the observed phenomena, it is well known that the increased amount of the weaker acidic sites over MgO modified ZSM-5 is due to the creation of Lewis acidic sites of $Mg(OH)^+$, which is formed by substituting $Mg^{2+}$ for the protons of hydroxyl groups [53,61]. Consequently, the amount of the stronger Brønsted acid is sharply decreased with increasing MgO loadings as a result of the consumption of the protons. Considering the difference in reactivity of the Brønsted protons, as indicated in reference [53], the amount of the weaker Brønsted acidic sites is expected to decrease at a higher loading of MgO over H-ZSM-5. Thus, the observed maximum of the weaker acidic sites over H-ZSM-5 with 1.41–2.92 wt.% MgO loadings is well explained if the opposite changing trends of the weaker Lewis and Brønsted acids with increasing MgO loadings are considered. Moreover, the slightly decreased amount of weaker acidic sites at higher MgO loadings (>2.92 wt.%) can be reasonably ascribed to the consumption of the protons of hydroxyl groups.

### 3.3. SRD performance

#### 3.3.1. Catalytic results

To reveal the impact of the acidic catalyst on the performance of SRD, the parent and MgO-modified H-ZSM-5 were applied to prepare the bifunctional catalyst under the same conditions, and the time-on-stream (TOS) results of SRD are given in Fig. 6. As indicated in Fig. 6a, the initial DME conversion over H-ZSM-5 based bifunctional catalyst was 100%, but was clearly decreased with increasing TOS (~90% at TOS of 6 h). On the contrary, stable DME conversions of ~60–95% were obtained over the MgO modified H-ZSM-5 catalysts, and a generally decreased DME conversion with increasing MgO loading was observed. Specifically, the H-ZSM-5 modified with 0.61, 1.41, and 1.98 wt.% MgO showed almost the same DME conversion of above 95% while only about 60% DME conversion was obtained in the case of the 8.16 wt.% MgO loaded sample. Thus, a strong dependence of DME conversion on the content of MgO over H-ZSM-5 was clearly manifested. As shown in Fig. 6b, the $H_2$ yield was continuously increased from ~80 to 93% with increasing the content of MgO from 0.61–1.98 wt.%. After this, the further increase of MgO content until 8.16 wt.% led to a significant decrease of $H_2$ yield to ~60%, which is much lower than that over the parent H-ZSM-5 (~73%). When the carbon-containing products were examined, as given in Fig. 6c, the selectivity of $CH_4$ and methanol was low, and the most abundant product was $CO_2$ (about 80–97% selectivity). Moreover, the selectivity of $C_2$-$C_4$ hydrocarbons was significantly decreased from about 16% over the parent H-ZSM-5 to about 0.6% over the 1.98 wt.% MgO modified H-ZSM-5, and the further increase of MgO loading until 8.16 wt.% led to a constant low selectivity of $C_2$-$C_4$ hydrocarbons (less than 0.5%). These results indicate that a high-performance acidic catalyst for SRD can be obtained by the modification of H-ZSM-5 with MgO, and the optimal MgO loading is determined to be 1.98 wt.%.

#### 3.3.2. Discussion

For the studied bifunctional catalysts, the same $Cu/ZnO/Al_2O_3$ was used. Moreover, all the parameters for the preparation of the bifunctional catalyst were kept the same except the acidic catalyst used. Keeping these facts in mind, the observed SRD results can be well explained based on the SRD mechanism and the characterization results of the catalyst, and are discussed as follows.

According to the two-step mechanism of SRD [7], DME is hydrolyzed to methanol (Eq. (2)) catalyzed by the acidic zeolite, and then the produced methanol is reformed with steam on Cu-based catalyst to give $CO_2$ and $H_2$ (Eq. (3)). Following this mechanism, the low selectivity of methanol (<5%) over all the bifunctional catalysts suggests that the commercial $Cu/ZnO/Al_2O_3$ is very active for SRM, leading to the high $CO_2$ selectivity. Although RWGS reaction can be catalyzed by the $Cu/ZnO/Al_2O_3$, it is not favored as a result of the relatively low reaction temperature of 290 °C, leading to the very low CO selectivity (less than 1%) over the bifunctional catalyst containing H-ZSM-5. The slight increase of CO selectivity with increasing MgO loading from 0.61 to 1.98 wt.% can be ascribed to the promotional effect of MgO on RWGS reaction since it has long been investigated as a catalyst/promoter for water-gas shift reaction [63]. Apparently, it seems that the clearly decreased CO selectivity with increasing MgO loading from 2.92 to 8.16 wt.% is contradictory to this explanation. However, as a result of the significantly decreased DME conversion at higher MgO loadings, the RWGS reaction is shifted backward, leading to the decreased CO selectivity.

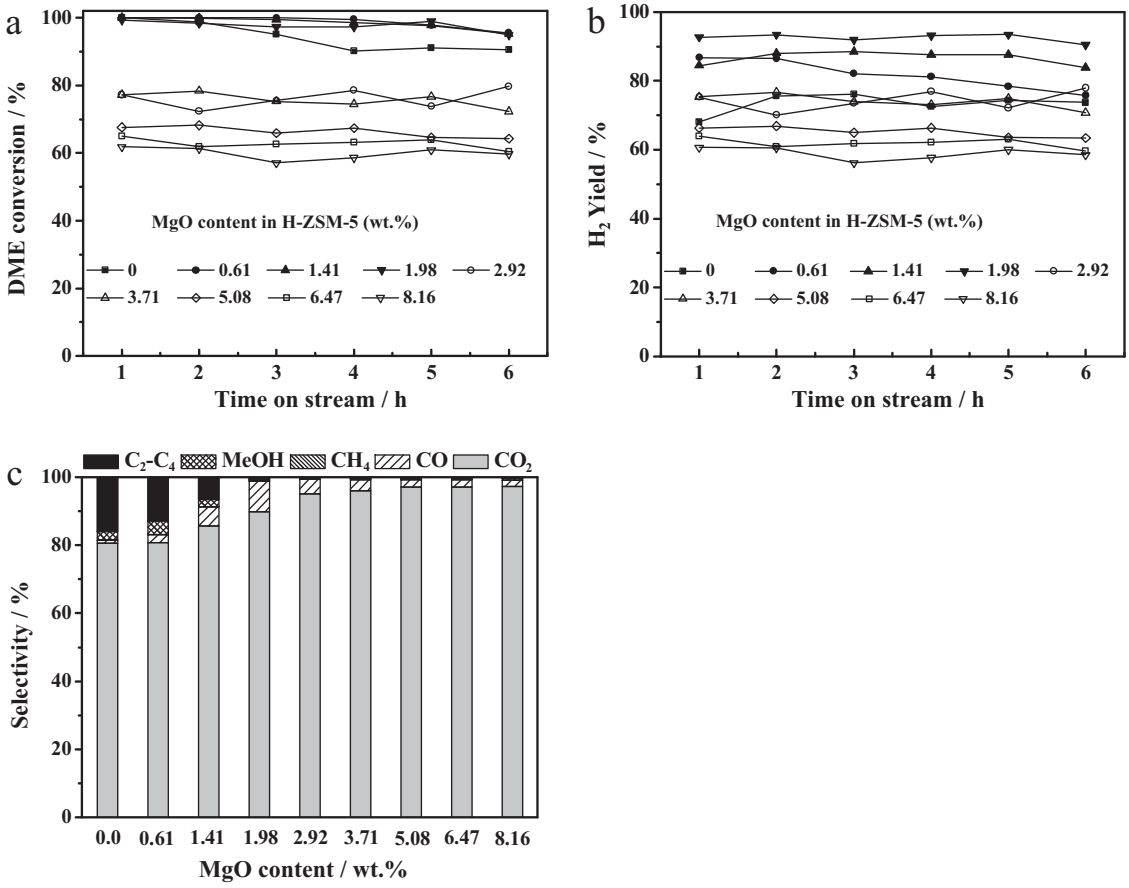


**Fig. 6.** SRD results over different bifunctional catalysts (0.45 g Cu/ZnO/$Al_2O_3$ + 0.45 g H-ZSM-5 modified with different contents of MgO) as a function of TOS under the conditions of $T$ = 290 °C, $P$ = 1 atm, GHSV = 4000 $h^{-1}$ (a: DME conversion; b: $H_2$ yield; c: Selectivity of carbon-containing products at TOS of 4 h).

If stronger acidic sites are present over the catalyst, as usually do in zeolites, DME to hydrocarbon (DTH, Eq. (8)) and methanol to hydrocarbon (MTH, Eq. (9)) will take place as side reactions of SRD, which has been observed in many works [36–42]. Thus, as a result of the stronger acidic sites over the parent H-ZSM-5 (Fig. 5), the clearly decreased DME conversion with increasing TOS (Fig. 6a) can be reasonably ascribed to the coke deposition from the side reactions of DTH (Eq. (8)) and MTH (Eq. (9)), which is consistent to the previous reports [37,39]. Furthermore, this is also supported by the facts that (1) the black color of H-ZSM-5 in the used catalyst is evident of coke deposition; (2) $C_2$-$C_4$ hydrocarbons with a selectivity of about 16% are formed in the SRD products.

In the cases of MgO-modified H-ZSM-5, as revealed in Sections 3.1.1 and 3.1.2, MgO is highly dispersed on the surface of H-ZSM-5, and very limited effect of MgO on the structural properties of the zeolite is observable irrespective of the MgO loadings. Moreover, when DME conversion and $H_2$ yield (Fig. 6) are correlated with the surface area or pore volume of the MgO-modified H-ZSM-5 (Table 1), it can be concluded that the impact of these textural properties on the SRD performance of different bifunctional catalysts is negligible. On the contrary, in comparison with the parent H-ZSM-5, the amount of the stronger acidic sites was sharply decreased with increasing MgO loadings (Fig. 5). Moreover, the activity of Lewis acids such as alumina is very low for the DME hydrolysis at the reaction temperature of 290 °C since much higher temperature is required for SRD over alumina-based catalysts [34–40]. Thus, combining these two points, the two-step mechanism of SRD, and the results and discussion on the acidic properties of the MgO-modified H-ZSM-5 (Section 3.2), the clearly lower DME conversion over the catalyst with MgO loadings above 2.92 wt.% can be well explained as the significantly decreased amount of the stronger acidic sites. Because that the stronger acidic sites are favorable for the DTH and MTH reactions, this explanation can also be applied to explain the greatly decreased selectivity of $C_2$-$C_4$ hydrocarbons with increasing MgO loadings over H-ZSM-5 (Fig. 6c). When the maximum $H_2$ yield over 1.98 wt.% MgO-modified H-ZSM-5 is concerned, it is determined by the opposite factors of (1) the significantly decreased selectivity of $C_2$-$C_4$ hydrocarbons with increasing MgO loading from 0.61 to 2.92 wt.% (Fig. 6c); (2) greatly decreased DME conversion in the cases with a MgO loading of ≥2.92 wt.%

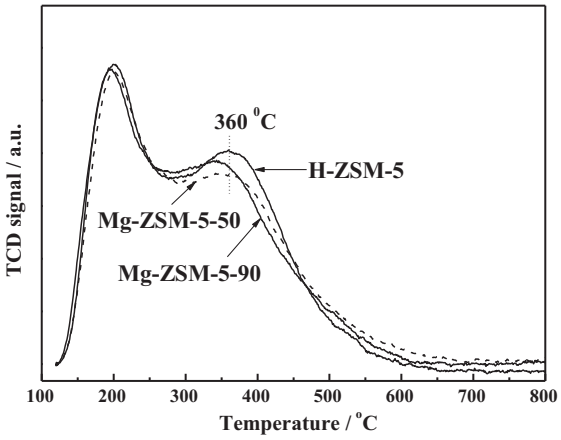


**Fig. 7.** $NH_3$-TPD profiles of the parent H-ZSM-5 and the $Mg^{2+}$-exchanged ZSM-5.

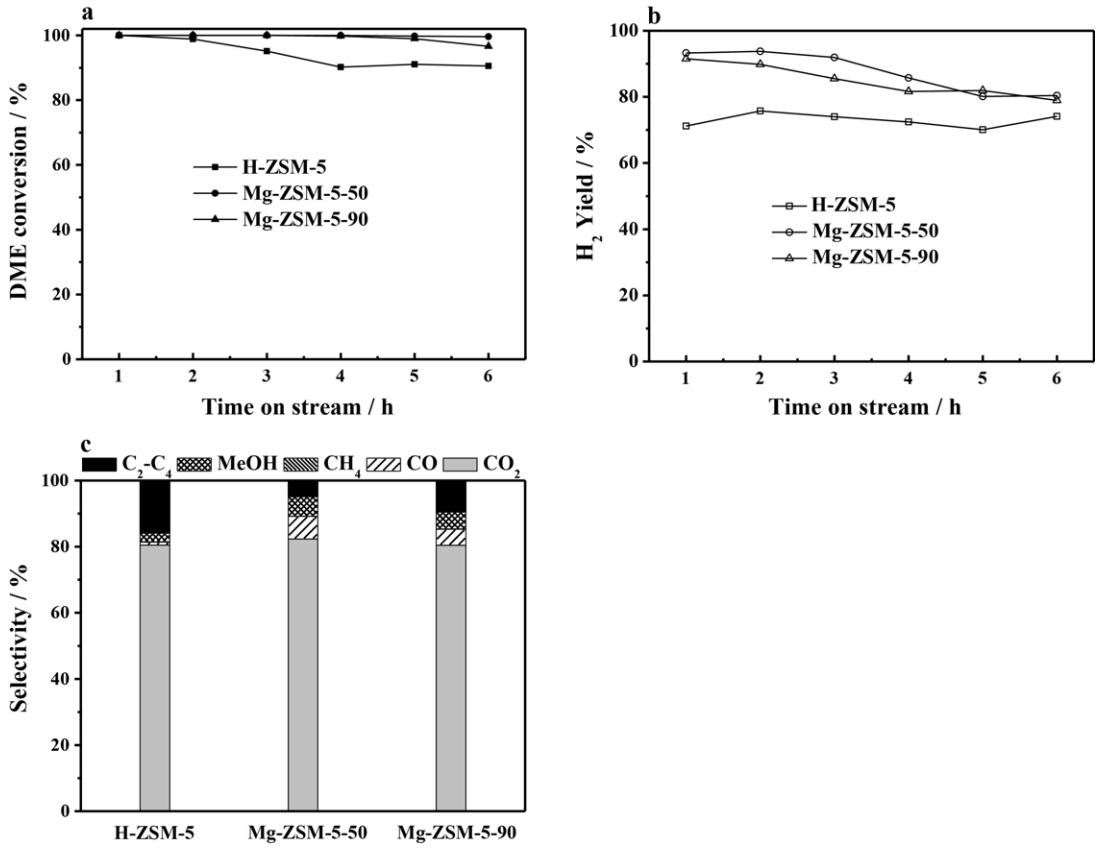


**Fig. 8.** The TOS DME conversion (a), $H_2$ yield (b), and selectivity of carbon-containing products at TOS of 4 h (c) over the bifunctional catalysts of 0.45 g $Cu/ZnO/Al_2O_3$ + 0.45 g zeolite under the conditions of $T = 290\,^{\circ}C$, $P = 1$ atm, GHSV = 4000 $h^{-1}$.

(Fig. 6c). Thus, the effect of MgO on the SRD results is mainly determined by the impact of MgO on the acidic properties of H-ZSM-5.

From the above discussion, it is inferred that the property of the stronger acidic sites over H-ZSM-5 is a critical parameter to determine the SRD performance. To further confirm this, the same H-ZSM-5 was ion-exchanged with $Mg^{2+}$ (0.04 mol/$dm^3$ $Mg(NO_3)_2$ solution) at 50 and 90 °C for 8 h, and abbreviated as Mg-ZSM-5-50 and Mg-ZSM-5-90, respectively. After washing with de-ionized water, drying at 120 °C for 12 h, and calcining in air at 550 °C for 3 h, the same procedure to that of the MgO impregnated H-ZSM-5 was applied for the preparation of the bifunctional catalyst. Results indicate that the influence of the $Mg^{2+}$-exchange on the structure of H-ZSM-5 was not observable from the XRD patterns (not shown). From the $NH_3$-TPD results given in Fig. 7, H-ZSM-5, Mg-ZSM-5-50 and Mg-ZSM-5-90 showed almost the identical weaker acidic properties. However, slight changes were observed in the aspect of the stronger acidic sites. In comparison with the parent H-ZSM-5, Mg-ZSM-5-50 showed clearly lower peak intensity although the same $NH_3$-desorption peak temperature of about 360 °C was observed. For Mg-ZSM-5-90, however, the peak temperature for $NH_3$ desorption was slightly decreased to be ~340 °C. It is noteworthy that the changes of the acidic properties of the Mg-ZSM-5 were much less pronounced than those of the 0.61 wt.% MgO impregnated H-ZSM-5, which is agreeable with the common fact that the exchangeable protons in H-ZSM-5 cannot be efficiently replaced by $Mg^{2+}$ via an ion-exchange method. Thus, without clearly affecting other properties of the zeolite, a small part of the stronger acidic sites was selectively removed for the $Mg^{2+}$-exchanged H-ZSM-5. As indicated in Fig. 8, a more stable DME conversion within TOS of 6 h over Mg-ZSM-5 than H-ZSM-5 was obtained. Moreover, $H_2$ yield was clearly increased and selectivity of $C_2$-$C_4$ hydrocarbons was obviously decreased. When the $NH_3$-TPD results (Figs. 5 and 7) are considered, the SRD results given in Fig. 8 well support the explanation in the case by using MgO impregnated H-ZSM-5 as a solid acid. Moreover, the slightly higher selectivity of $C_2$-$C_4$ hydrocarbons over Mg-ZSM-5-90 than Mg-ZSM-5-50 can be reasonably ascribed to the small changes of the acidic strength as revealed from the peak temperatures for $NH_3$ desorption (Fig. 7).

## 4. Conclusions

Based on the results and discussion, the conclusions are drawn as follows. After loading 0.61–8.16 wt.% MgO via the incipient impregnating method, both the structure and crystallinity of H-ZSM-5 were well retained, and no magnesium species were detected by XRD. The highly dispersed MgO was revealed to be mainly in the internal surfaces of H-ZSM-5, leading to the continuously decreased BET surface area and pore volume by increasing the MgO loadings. The amount of the stronger acidic sites was sharply decreased after loading 0.61 wt.% MgO on H-ZSM-5, and it was continuously decreased when the MgO loading was further increased until 8.16 wt.%. On the contrary, the maximum amount of weaker acidic sites was observed over 1.41–2.92 wt.% MgO loaded samples. Moreover, irrespective of the MgO loadings, the strength of the weaker and stronger acidic sites was kept almost the same. By using the MgO-modified H-ZSM-5 as a solid acid for SRD, significant impact of the MgO loadings on DME conversion, $H_2$ yield, and selectivity of the carbon-containing products was observed. Over the optimized catalyst, about 93% hydrogen yield was obtained, and the side reactions for the formation of hydrocarbons were greatly inhibited. The reaction results were well explained based on the catalyst characterizations, and the property of the stronger acidic sites over the MgO-modified H-ZSM-5 was revealed to be a crucial

factor in determining the SRD performance of the bifunctional catalyst. The simple impregnation procedure and the high efficiency in versatile tailoring the acidity make MgO-modified H-ZSM-5 a practical, highly efficient, and promising solid acid for hydrogen production via SRD.

## Acknowledgments

The group of Shaanxi Normal University thanks the financial supports by Program for New Century Excellent Talents in University (NCET-08-0799), the Program for Changjiang Scholars and Innovative Research Team in University (IRT1070), and the Fundamental Research Funds for the Central Universities (GK201002043, 2010ZYGX013).

## References

[1] C. Bernay, M. Marchand, M. Cassir, Journal of Power Sources 108 (2002) 139–152.
[2] U. Eberle, M. Felderhoff, F. Schüth, Angewandte Chemie International Edition 48 (2009) 6608–6630.
[3] P.K. Cheekatamarla, C.M. Finnerty, Journal of Power Sources 160 (2006) 490–499.
[4] D.R. Palo, R.A. Dagle, J.D. Holladay, Chemical Reviews 107 (2007) 3992–4021.
[5] T.A. Semelsberger, R.L. Borup, H.L. Greene, Journal of Power Sources 156 (2006) 497–511.
[6] V.A. Sobyanin, S. Cavallaro, S. Freni, Energy and Fuels 14 (2000) 1139–1142.
[7] V.V. Galvita, G.L. Semin, V.D. Belyaev, T.M. Yurieva, V.A. Sobyanin, Applied Catalysis A-General 216 (2001) 85–90.
[8] T.A. Semelsberger, R.L. Borup, Journal of Power Sources 152 (2005) 87–96.
[9] T.A. Semelsberger, R.L. Borup, Journal of Power Sources 155 (2006) 340–352.
[10] K. Faungnawakij, R. Kikuchi, K. Eguchi, Journal of Power Sources 164 (2007) 73–79.
[11] K. Faungnawakij, N. Viriya-empikul, W. Tanthapanichakoon, International Journal of Hydrogen Energy 36 (2011) 5865–5874.
[12] K. Faungnawakij, K. Eguchi, Catalysis Surveys from Asia 15 (2011) 12–24.
[13] N. Shimoda, K. Faungnawakij, R. Kikuchi, K. Eguchi, International Journal of Hydrogen Energy 36 (2011) 1433–1441.
[14] K. Faungnawakij, N. Shimoda, N. Viriya-empikul, R. Kikuchi, K. Eguchi, Applied Catalysis B: Environmental 97 (2010) 21–27.
[15] S. Kudo, T. Maki, K. Miura, K. Mae, Carbon 48 (2010) 1186–1195.
[16] S. Park, H. Kim, B. Choi, Journal of Industrial and Engineering Chemistry 16 (2010) 734–740.
[17] M. Nilsson, K. Jansson, P. Jozsa, L.J. Pettersson, Applied Catalysis B: Environmental 86 (2009) 18–26.
[18] F. Solymosi, R. Barthos, A. Kecskeméti, Applied Catalysis A-General 350 (2008) 30–37.
[19] Y. Yamada, T. Mathew, A. Ueda, H. Shioyama, T. Kobayashi, Applied Surface Science 252 (2006) 2593–2597.
[20] G. Halasi, T. Bánsági, F. Solymosi, ChemCatChem 1 (2009) 311–317.
[21] C. Ledesma, J. Llorca, Journal of Physical Chemistry C 115 (2011) 11624–11632.
[22] C. Ledesma, U.S. Ozkan, J. Llorca, Applied Catalysis B: Environmental 101 (2011) 690–697.
[23] A. Gazsi, I. Ugrai, F. Solymosi, Applied Catalysis A-General 391 (2011) 360–366.
[24] X. Wang, X. Pan, R. Lin, S. Kou, W. Zou, J.-X. Ma, International Journal of Hydrogen Energy 35 (2010) 4060–4068.
[25] K. Faungnawakij, N. Shimoda, T. Fukunaga, R. Kikuchi, K. Eguchi, Applied Catalysis B: Environmental 92 (2009) 341–350.
[26] N. Shimoda, K. Faungnawakij, R. Kikuchi, T. Fukunaga, K. Eguchi, Applied Catalysis A-General 365 (2009) 71–78.
[27] K. Faungnawakij, R. Kikuchi, N. Shimoda, T. Fukunaga, K. Eguchi, Angewandte Chemie International Edition 47 (2008) 9314–9317.
[28] M. Yang, Y. Men, S. Li, G. Chen, Applied Catalysis A-General 433–434 (2012) 26–34.
[29] P.V. Snytnikov, S.D. Badmaev, G.G. Volkova, D.I. Potemkin, M.M. Zyryanova, V.D. Belyaev, V.A. Sobyanin, International Journal of Hydrogen Energy 37 (2012) 16388–16396.
[30] K. Takeishi, H. Suzuki, Applied Catalysis A-General 260 (2004) 111–117.
[31] S.D. Badmaev, G.G. Volkova, V.D. Belyaev, V.A. Sobyanin, Reaction Kinetics and Catalysis Letters 90 (2007) 205–211.
[32] T. Matsumoto, T. Nishiguchi, H. Kanai, K. Utani, Y. Matsumura, S. Imamura, Applied Catalysis A-General 276 (2004) 267–273.
[33] D. Feng, Y. Wang, D. Wang, J. Wang, Chemical Engineering Journal 146 (2009) 477–485.
[34] Y. Tanaka, R. Kikuchi, T. Takeguchi, K. Eguchi, Applied Catalysis B: Environmental 57 (2005) 211–222.
[35] T.A. Semelsberger, K.C. Ott, R.L. Borup, H.L. Greene, Applied Catalysis B: Environmental 61 (2005) 281–287.
[36] T.A. Semelsberger, K.C. Ott, R.L. Borup, H.L. Greene, Applied Catalysis B: Environmental 65 (2006) 291–300.
[37] T.A. Semelsberger, K.C. Ott, R.L. Borup, H.L. Greene, Applied Catalysis A-General 309 (2006) 210–223.
[38] T. Fukunaga, N. Ryumon, S. Shimazu, Applied Catalysis A-General 348 (2008) 193–200.
[39] K. Faungnawakij, Y. Tanaka, N. Shimoda, T. Fukunaga, S. Kawashima, R. Kikuchi, K. Eguchi, Applied Catalysis A-General 304 (2006) 40–48.
[40] K. Faungnawakij, R. Kikuchi, T. Matsui, T. Fukunaga, K. Eguchi, Applied Catalysis A-General 333 (2007) 114–121.
[41] T. Kawabata, H. Matsuoka, T. Shishido, D. Li, Y. Tian, T. Sano, K. Takehira, Applied Catalysis A-General 308 (2006) 82–90.
[42] J. Li, Q.-J. Zhang, X. Long, P. Qi, Z.-T. Liu, Z.-W. Liu, Chemical Engineering Journal 187 (2012) 299–305.
[43] T. Nishiguchi, K. Oka, T. Matsumoto, H. Kanai, K. Utani, S. Imamura, Applied Catalysis A-General 301 (2006) 66–74.
[44] K. Oka, T. Nishiguchi, H. Kanai, K. Utani, S. Imamura, Applied Catalysis A-General 309 (2006) 187–191.
[45] N. Shimoda, K. Faungnawakij, R. Kikuchi, K. Eguchi, Applied Catalysis A-General 378 (2010) 234–242.
[46] J. Vicente, A.G. Gayubo, J. Ereña, A.T. Aguayo, M. Olazar, J. Bilbao, Applied Catalysis B: Environmental 130–131 (2013) 73–83.
[47] Y.-G. Li, H. Jun, Applied Catalysis A-General 142 (1996) 123–137.
[48] X. Guo, J. Shen, L. Sun, C. Song, X. Wang, Applied Catalysis A-General 261 (2004) 183–189.
[49] Z. Zhao, W. Qiao, X. Wang, G. Wang, Z. Li, L. Cheng, Microporous and Mesoporous Materials 94 (2006) 105–112.
[50] B. Mitra, D. Kunzru, Catalysis Letters 141 (2011) 1569–1579.
[51] B. Xue, Y. Li, L. Deng, Catalysis Communications 10 (2009) 1609–1614.
[52] H. Li, M. Li, Y. Chu, H. Nie, Microporous and Mesoporous Materials 117 (2009) 635–639.
[53] D. Mao, W. Yang, J. Xia, B. Zhang, Q. Song, Q. Chen, Journal of Catalysis 230 (2005) 140–149.
[54] B. Li, S. Li, N. Li, H. Chen, W. Zhang, X. Bao, B. Lin, Microporous and Mesoporous Materials 88 (2006) 244–253.
[55] H. Wang, H. Guan, L. Duan, Y. Xie, Catalysis Communications 7 (2006) 802–806.
[56] P. Kovacheva, A. Predoeva, K. Arishtirova, S. Vassilev, Applied Catalysis A-General 223 (2002) 121–128.
[57] Y.-C. Xie, Y.-Q. Tang, in: D.D. Eley, H. Pines, P.B. Weisz (Eds.), Advances in Catalysis, Academic Press, Inc., New York, 1990, pp. 1–43.
[58] F. Lónyi, J. Valyon, Microporous and Mesoporous Materials 47 (2001) 293–301.
[59] S.G. Zhang, S. Higashimoto, H. Yamashita, M. Anpo, Journal of Physical Chemistry B 102 (1998) 5590–5594.
[60] D. Dumitriu, R. Bârjega, L. Frunza, D. Macovei, T. Hu, Y. Xie, V.I. Pârvulescu, S. Kaliaguine, Journal of Catalysis 219 (2003) 337–351.
[61] Y.-G. Li, W.-H. Xie, S. Yong, Applied Catalysis A-General 150 (1997) 231–242.
[62] M. Iwasaki, K. Yamazaki, K. Banno, H. Shinjoh, Journal of Catalysis 260 (2008) 205–216.
[63] T. Shido, Y. Iwasawa, Journal of Catalysis 136 (1992) 493–503.